International Journal of Biological Macromolecules

Research article

First crystal structure of an NADP$^+$-dependent L-arginine dehydrogenase belonging to the μ-crystallin family

Ryushi Kawakami[a], Naoki Takami[b], Junji Hayashi[a], Kazunari Yoneda[c], Taketo Ohmori[d], and Toshihisa Ohshima[d], and Haruhiko Sakuraba[b, *]

[a]Division of Bioscience and Bioindustry, Graduate School of Technology, Industrial and Social Sciences, Tokushima University, 2-1, Minamijosanjima-cho, Tokushima, Tokushima 770-8513, Tokushima, Japan

[b]Department of Applied Biological Science, Faculty of Agriculture, Kagawa University, 2393 Ikenobe, Miki-cho, Kita-gun, Kagawa 761-0795, Japan

[c]Department of Food and Life Sciences, School of Agriculture, Tokai University, 871-12 Sugido, Mashiki-machi, Kamimashiki-gun, Kumamoto 861-2205, Japan

[d]Department of Biomedical Engineering, Faculty of Engineering, Osaka Institute of Technology, 5-16-1 Ohmiya, Asahi-ku, Osaka 535-8585, Japan

* Corresponding author

E-mail address: sakuraba.haruhiko@kagawa-u.ac.jp (H. Sakuraba)

Highlights

- The crystal structure of an L-arginine dehydrogenase belonging to the μ-crystallin family was determined.
- The substrate recognition residues of L-arginine dehydrogenase notably differ from those predicted for L-alanine dehydrogenase.
- This study provides the first structural insight into the substrate binding mode of L-arginine dehydrogenase.

Abstract

Crystal structures of *Pseudomonas veronii* L-arginine dehydrogenase (L-ArgDH), belonging to the μ-crystallin/ornithine cyclodeaminase family, were determined for the enzyme in complex with L-lysine and $NADP^+$ and with L-arginine and NADPH. The main chain coordinates of the *P. veronii* L-ArgDH monomer showed notable similarity to those of *Archaeoglobus fulgidus* L-AlaDH, belonging to the same family, and *Pro*-R specificity similar to L-AlaDH for hydride transfer to $NADP^+$ was postulated. However, the residues

recognizing the α-amino group of the substrates differed between the two enzymes. Based on a substrate modeling study, it was proposed that in *A. fulgidus* L-AlaDH, the amino group of L-alanine interacts via a water molecule (W510) with the side chains of Lys41 and Arg52. By contrast, the α-amino group of L-arginine formed hydrogen bonds with the side chains of Thr224 and Asn225 in *P. veronii* L-ArgDH. Moreover, the guanidino group of L-arginine was fixed into the active site via hydrogen bonds with the side chain of Asp54. Site-directed mutagenesis suggested that Asp54 plays an important role in maintaining high reactivity against the substrate and that Tyr58 and Lys71 play critical roles in enzyme catalysis.

Keywords:

L-arginine dehydrogenase, μ-crystallin/ornithine cyclodeaminase family, crystal structure, amino acid dehydrogenase, site-directed mutagenesis

1. Introduction

Amino acid dehydrogenases, which catalyze $NAD(P)^+$-dependent dehydrogenation at the α-carbon (C2) position of amino acids accompanied by deamination, can be classified into several superfamilies. For example, bacterial L-alanine dehydrogenases (L-

AlaDH, EC1.4.1.1) appear similar to the family of D-2-hydroxyacid dehydrogenases [1] but, with respect to amino acid sequence and 3D structure, stand apart from the ELFVW superfamily, which includes L-glutamate dehydrogenase (EC1.4.1.2-4) [2], L-leucine dehydrogenase (EC1.4.1.9) [3], L-phenylalanine dehydrogenase (L-PheDH, EC1.4.1.20) [4], L-valine dehydrogenase (EC1.4.1.8) [5], and L-tryptophan dehydrogenase (EC1.4.1.19) [6, 7]. Whereas ELFVW superfamily enzymes show *Pro*-S stereospecificity in the hydride transfer from NAD(P)H to oxo acid, bacterial L-AlaDH [1] shows *Pro*-R stereospecificity. L-Aspartate dehydrogenases (EC1.4.1.21) observed in the hyperthermophilic bacterium *Thermotoga maritima* [8] and hyperthermophilic archaeon *Archaeoglobus fulgidus* [9, 10] show *Pro*-R stereospecificity in the hydride transfer from NAD(P)H and share no structural similarity with either ELFVW superfamily enzymes or other families that include bacterial L-AlaDH. On the contrary, those enzymes have low similarity to the structures of aspartate semialdehyde dehydrogenase, inositol 1-phosphate synthase, and dihydrodipicolinate dehydrogenase [8]. Moreover, a fourth superfamily of amino acid dehydrogenases is represented by the L-AlaDH from *A. fulgidus*, which differs from many bacterial L-AlaDHs, despite exhibiting the same catalytic activity and showing *Pro*-R specificity [11, 12]. That enzyme was initially annotated as an ornithine cyclodeaminase (OCD) based on the high sequence homology with the μ-crystallin/OCD

protein family.

NAD(P)$^+$-dependent L-arginine dehydrogenase (EC 1.4.1.25, L-ArgDH) was recently identified as a novel amino acid dehydrogenase belonging to the μ-crystallin/OCD family [13]. L-ArgDH was first observed in *Pseudomonas aeruginosa* PAO1, an opportunistic human pathogen, and was found to function together with FAD-dependent D-arginine dehydrogenase to convert D-arginine to L-arginine through its oxo-analog, 5-guanidino-2-oxopentanoate [13]. When the *P. aeruginosa* gene *DauB*, encoding L-ArgDH, was expressed in *Escherichia coli*, the product catalyzed the NAD$^+$-dependent deamination of L-arginine to 5-guanidino-2-oxopentanoate. However, the molecular and catalytic properties of *P. aeruginosa* L-ArgDH have yet to be reported owing to the enzyme's instability. Recently, a gene homolog (*PverR02_12350*) of *DauB* was identified in genomic data from the nonpathogenic bacterium *P. veronii* JCM 11942 [14]. Its product possesses 67.8% amino acid sequence homology with *P. aeruginosa* L-ArgDH and exhibits strong NADP$^+$-dependent L-ArgDH activity. Because this enzyme is stable in the presence of 10% (v/v) glycerol, its enzymatic properties have been analyzed in detail. The most notable characteristic of this enzyme is its high substrate specificity for L-arginine. D-Arginine, L-lysine, L-ornithine, L-citrulline, L-leucine, L-phenylalanine, L-histidine, L-glutamate, glycine and L-alanine are all inert as electron

donors. *A. fulgidus* L-AlaDH is not substrate-specific; L-valine, L-serine, L-threonine, L-aspartate, and L-isoleucine can also serve as substrates but at rates 12% or less of that for L-alanine [12]. The crystal structure of *A. fulgidus* L-AlaDH complexed with NAD^+ has been determined, and modeling of substrate L-alanine into the active site has been reported [11]. Structural analysis of *P. veronii* L-ArgDH may shed light on the substrate-recognition mechanism of this enzyme, which specifically acts on L-arginine.

In the present study, therefore, we determined the molecular structures by protein crystallography of the inactive *P. veronii* L-ArgDH complex with L-lysine and coenzyme $NADP^+$ bound and the abortive enzyme complex with its natural substrate, L-arginine, and NADPH bound. We then compared the architecture of the active site with that of *A. fulgidus* L-AlaDH and *P. putida* OCD [15]. This is the first description of the structure of an L-ArgDH belonging to the μ-crystallin/OCD family.

2. Experimental procedures

2.1. Purification of the recombinant enzyme

The recombinant enzyme was produced using the expression plasmid pET21a-L-ArgDH, and it was purified as previously described [14] with minor modifications. *E. coli* BL21 (DE3) CodonPlus RIPL (Stratagene, Tokyo, Japan) cells harboring pET21a-L-

ArgDH were cultivated [14], and gene expression was induced by incubating the cells with isopropyl-β-D-thiogalactopyranoside (final 0.1 mM) for 3 h. The cells were then collected by centrifugation (6,000 ×g, 10 min), suspended in 20 mM NaH_2PO_4-Na_2HPO_4 buffer (Buffer A, containing 10% (v/v) glycerol, 0.5 M NaCl, 0.01% (v/v) 2-mercaptoethanol, and 5 mM imidazole; pH 7.2), and disrupted by sonication. After centrifugation (12,000 ×g, 10 min), the resultant crude extract was applied to a Protino Ni-IDA column (Macherey-Nagel, Germany) equilibrated with Buffer A, and the column was washed with the same buffer. The enzyme was eluted with a linear gradient of 5-500 mM imidazole in Buffer A. The L-ArgDH-containing fractions were analyzed using SDS-PAGE, pooled, and concentrated by ultrafiltration (Amicon Ultra 30K NMWL; Millipore, Tokyo). The enzyme solution was then loaded onto a HiLoad 26/60 Superdex 200 gel-filtration column (Cytiva, Marlborough, MA, USA) equilibrated with 20 mM NaH_2PO_4-Na_2HPO_4 buffer (pH 7.2) containing 10% (v/v) glycerol and eluted with the same buffer. Column chromatography was performed at room temperature using a BioLogic Duo Flow fast protein liquid chromatography system (Bio-Rad, Tokyo). Expression and purification of mutant enzymes were performed using the same method used for wild-type enzymes, except that the gel-filtration step was omitted for purification.

2.2. Determination of enzyme activity and protein concentration

Enzyme activity was assayed spectrophotometrically using a Shimadzu UV-1280 spectrophotometer (Shimadzu, Kyoto, Japan) equipped with a thermostat. The standard assay for L-ArgDH activity was performed as previously described [14] with minor modifications. The standard reaction mixture comprised 200 mM glycine-NaOH buffer (pH 9.5), 1.25 mM $NADP^+$, 10 mM L-arginine, and the enzyme in a final volume of 1.0 mL. The mixture without the enzyme was incubated at 27°C for 3 min in a cuvette with a 1.0-cm light path length; the reaction was then initiated by addition of the enzyme. The NADPH concentration was monitored by measuring the absorbance at 340 nm (extinction coefficient ε = 6.22 mM^{-1} cm^{-1}). The protein concentration was determined using the Bradford method (Protein Assay Dye Reagent; Bio-Rad), with bovine serum albumin serving as the standard.

2.3. Site-directed mutagenesis

Site-directed mutagenesis was accomplished using a QuikChange Lightning site-directed mutagenesis kit (Agilent Technologies, Tokyo) according to the manufacturer's instructions. The expression vector pET21a-L-ArgDH served as the template; the primer

sets used are listed in Supplementary Table 1.

2.4. Crystallization and data collection

For the crystallization trial, the purified enzyme was concentrated to about 10 mg/mL using ultrafiltration. Crystals of *P. veronii* L-ArgDH with L-lysine and $NADP^+$ bound (an inactive complex) were obtained using the sitting drop vapor diffusion method, in which 1 μL of enzyme solution containing 5 mM L-lysine and 1 mM $NADP^+$ was mixed with an equal volume of mother liquor composed of 100 mM imidazole buffer (pH 8.0), 200 mM NaCl, and 30% (w/v) polyethylene glycol (PEG) 8,000. Initially, clustered crystals grew, which were then suspended in the mother liquor and crushed with Seed Bead (Hampton Research, Aliso Viejo, CA). A new drop was then inoculated with micro-seeds from the slurry according to the manufacturer's instructions. Diffraction-quality crystals were obtained following several cycles of seeding. Crystals of the abortive complex of enzyme with L-arginine and NADPH bound were grown in sitting drops composed of 1 μL of enzyme solution containing 5 mM L-arginine and 1 mM NADPH mixed with an equal volume of mother liquor composed of 70 mM sodium acetate buffer (pH 4.6), 5.6% (w/v) PEG4,000, and 30% (v/v) glycerol. In all cases, the sitting drops were equilibrated against 0.1 mL of mother liquor, and the crystals were grown for one

week at 20°C.

Data were collected using a Dectris Pilatus3 S6M detector system on the BL5A beamline at the Photon Factory, Tsukuba, Japan. The measurements were conducted on a crystal cooled to 100 K in a stream of nitrogen gas. For crystals of the Lys-$NADP^+$-enzyme complex, mother liquor containing 30% (v/v) ethylene glycol was used for cryoprotection. The mother liquor for crystals of the L-arginine-NADPH-enzyme complex already contained 30% (v/v) glycerol, which was directly used for cryoprotection. The data were processed using XDS [16], followed by Aimless [17] in the CCP4 [18] program suite.

2.4. Phasing, refinement, and structure analysis

The structure of the Lys-$NADP^+$-enzyme complex was solved to a resolution of 2.2 Å with molecular replacement using MOLREP [19] in the CCP4 [18] program suite. The structure of the monomer predicted using AlphaFold2 [20] served as the search model. Data in the resolution range of 46.7-3.0 Å were used for molecular replacement. Model building was performed using the program Coot [21]. Maximum-likelihood refinement at 2.2 Å resolution was performed using REFMAC5 [22]. NCS restraints were imposed during initial refinement. After several cycles of inspection of the 2Fo-Fc and Fo-Fc

density maps, the model was rebuilt; R = 0.213 (R_{free} = 0.260) in the final refined model. The structure of the L-arginine-NADPH-enzyme complex was solved to a resolution of 2.5 Å with molecular replacement using MOLREP [19]. The structure of chain A from the 2.2 Å model was used as a search model. Data in the resolution range 47.8-3.0 Å were used for molecular replacement. The model was then rebuilt using Coot [21], and refinement at the maximum resolution was performed using REFMAC5 [22] as described for the enzyme with L-lysine and $NADP^+$ bound; R = 0.228 (R_{free} = 0.274) in the final model. In all cases, water molecules were incorporated using Coot [21], and the model geometry was analyzed using MolProbity [23]. The data collection and refinement statistics are listed in Table 1.

Accessible surface areas (ASAs; radius of the probe solvent molecule = 1.4 Å) of the protein were calculated using the Proteins, Interfaces, Structures, and Assemblies (PISA) web server [24]. Hydrogen bonds were identified using CCP4mg [25]. For superposition of the structures, secondary-structure matching [26] was performed using Coot [21]. Molecular graphics figures were created using PyMOL (http://www.pymol.org/). The final Fo-Fc omit electron density maps were generated using Polder Maps [27] in the PHENIX program suite [28]. The atomic coordinates and structure factors have been deposited in the Protein Data Bank (PDB)

(http://www.rcsb.org/; IDs: 8J1C and 8J1G).

3. Results and Discussion

3.1. Overall structure of P. veronii L-ArgDH complexed with L-lysine and NADP$^+$

The L-ArgDH molecular structure complexed with L-lysine and NADP$^+$ was refined to a resolution of 2.2 Å (Table 1). The asymmetric unit comprised two homodimers with a solvent content of 51.2%, corresponding to a Matthew's coefficient [29] of 2.52 Å^3 Da^{-1}. The crystal structure indicated that the quaternary structure of *P. veronii* L-ArgDH was a dimer generated with a crystallographic twofold axis (Fig. 1). Oligomerization state analysis using PISA [24] confirmed the dimeric arrangement of *P. veronii* L-ArgDH, which is consistent with the subunit assembly of the enzyme estimated using gel filtration and SDS-PAGE (native enzyme, 66 kDa; subunit, 34 kDa) [14]. The model contained amino acid residues 4-77, 82-165, 170-283, and 288-315 in subunit A; 4-164, 168-177, 181-284, and 291-315 in subunit B; 4-283 and 287-315 in subunit C; and 4-164, 169-178, and 181-315 in subunit D, as well as three NADP$^+$, three imidazole, one ethylene glycol, one L-lysine, and 233 water molecules. Only subunit B had both the L-lysine and NADP$^+$ molecules bound (Supplementary Fig. 1). The structures of subunits A and D were the NADP$^+$-bound form, while that of subunit C was the L-lysine/NADP$^+$ unbound form.

PISA analysis showed that subunit B had the smallest ASA (13,170 Å^2), while subunit C had the largest ASA (13,850 Å^2). The ASAs for subunits A and D were 13,600 Å^2 and 13,630 Å^2, respectively. The protein packing in the crystals may account for the difference in the ASA among the subunits.

When the monomer model was uploaded to the DALI server [30] to identify proteins with similar structures (accessed on March 13, 2023), the amino acid dehydrogenase with the highest structural similarity was *A. fulgidus* L-AlaDH [PDB code: 1OMO (NAD^+-bound structure); root mean square deviation (r.m.s.d) = 2.4-2.5] [11]. The main chain coordinates of the *P. veronii* L-ArgDH monomer were similar to those of *A. fulgidus* L-AlaDH, as was the dimeric arrangement. The subunit folded into two domains: a small dimerization/catalytic domain 1 and a large NADP-binding domain 2 (Fig. 1).

3.2. $NADP^+$ and L-lysine binding sites

In *P. veronii* L-ArgDH subunit D (or A), the binding mode of the $NADP^+$ molecule was similar to that of the NAD^+ molecule in the structure of *A. fulgidus* L-AlaDH (Fig. 2A). The adenine ring of $NADP^+$ was recognized by the side chains of Pro161, Thr201, Ser203, and Val207, mainly via hydrophobic interactions. The adenine ribose phosphate formed hydrogen bonds with the main chain amide and the side chain of Ser162 in

addition to the side chain of Ser160 (the observed hydrogen bonds between the enzyme and $NADP^+$ are listed in Supplementary Table 2). The C3 hydroxyl group (O3B) of the adenine ribose formed hydrogen bonds with the side chain O and the main chain N atoms of Ser136. The pyrophosphate moiety formed hydrogen bonds with the main chain N atoms of Lys138 and Val139. The C2 hydroxyl group (O2D) of the nicotinamide ribose formed hydrogen bonds with the main chain N atoms of Thr224 and Asn225. The nicotinamide ring was fixed in a pocket formed by residues Arg111, Thr112, Ile222, and Ile297, and nicotinamide was recognized by the side chain of Arg111 and the main chain O atom of Ile222. In *A. fulgidus* L-AlaDH, the C2 and C3 hydroxyl groups (O2B and O3B) of the adenine ribose of NAD^+ formed hydrogen bonds with the side chains of Asp157 and Arg159 (Fig. 2B). In *P. veronii* L-ArgDH, these residues were replaced by Ser160 and Ser162, respectively (Supplementary Fig. 2A), whose side chains fix the C2 phosphate group of the adenine ribose of $NADP^+$. This change may be responsible for the difference in the cofactor preference between the two enzymes. *A. fulgidus* L-AlaDH is specific for NAD^+ [12], whereas *P. veronii* L-ArgDH prefers $NADP^+$ (four times higher specific activity) over NAD^+ [14].

The main chain coordinates of subunit D with $NADP^+$ bound were nearly identical to those of subunit B with L-lysine/$NADP^+$ bound (backbone r.m.s.d. = 0.73 Å). However,

a clear difference was observed for the mode of cofactor binding to the two subunits. In subunit B, the nicotinamide ribose, pyrophosphate, adenine phosphoribose, and adenine moieties of $NADP^+$ occupied positions similar to those observed for $NADP^+$ in subunit D (Supplementary Fig. 3). By contrast, the nicotinamide moiety of $NADP^+$ was found to be rotated by about 124° in an anticlockwise direction around C1D of $NADP^+$ relative to subunit D and was recognized by the side chain O and main chain N atoms of Thr109 (Supplementary Fig. 3).

The structure of *A. fulgidus* L-AlaDH in complex with NAD^+ has been determined with substrate L-alanine modeled into the active site [11]. It was expected that the carboxylate group of the substrate would be coordinated by an Arg (or Lys) side chain, as is observed in other amino acid dehydrogenase structures. The best candidate for the active site of *A. fulgidus* L-AlaDH was Arg108, and placement of L-alanine was performed considering the formation of a bidentate salt-link interaction with the side chain of Arg108. In this model, the amino group of L-alanine forms hydrogen bonds with the side chains of Lys41 and Arg52 via a water molecule (W510).

When the structure of *A. fulgidus* L-AlaDH was superimposed on that of *P. veronii* L-ArgDH subunit B, the amino acid residues involved in L-lysine binding differed from those proposed for the L-alanine molecule (Fig. 3). The epsilon amino group of L-lysine

was recognized by the side chain OH group of Tyr58 and the main chain O atom of Ile297, and the Cα amino group interacted via a water molecule (W200) with the main chain O atom of His105 (Supplementary Table 2). No interactions were observed between the carboxylate group of L-lysine and the enzyme, although Arg108 in *A. fulgidus* L-AlaDH was conserved as Arg111 (Supplementary Fig. 2A). The binding modes of L-lysine and $NADP^+$ to subunit B were insufficient for catalysis, which may relate to the inability of the enzyme to utilize L-lysine as a substrate.

3.3. Overall structure of P. veronii L-ArgDH complexed with L-arginine and NADPH

To further analyze its mode of substrate binding, we determined the structure of *P. veronii* L-ArgDH with its natural substrate, L-arginine, and NADPH bound (an abortive complex). The structure was refined to a resolution of 2.5 Å (Table 1), and the asymmetric unit consisted of two homodimers with a solvent content of 60.7%, corresponding to a Matthew's coefficient [29] of 3.1 $Å^3$ Da^{-1}. Subunit assembly was the same as that described for the enzyme with L-lysine and $NADP^+$ bound. The model contained amino acid residues 4-77 and 82-315 in subunit A; 4-315 in subunit B; 4-77, 82-164, and 180-315 in subunit C; and 4-164 and 171-315 in subunit D, as well as four NADPH, two ethylene glycol, four L-arginine, and 45 water molecules. Both the L-arginine and

NADPH molecules were observed in all subunits (Supplementary Fig. 4).

3.4. NADPH and L-arginine binding sites

The main chain coordinates of a *P. veronii* L-ArgDH monomer (subunit A) with L-arginine and NADPH bound were nearly identical to those of the enzyme with $NADP^+$ bound (subunit D with L-lysine and $NADP^+$ bound; backbone r.m.s.d. = 0.74 Å), as were the interactions between the enzyme and coenzyme. Superposition of the *A. fulgidus* L-AlaDH structure with NAD^+ bound onto that of *P. veronii* L-ArgDH with L-arginine/NADPH bound showed that the NADPH molecule in the latter was positioned/configured nearly identically to the NAD^+ molecule in the former. This suggests *P. veronii* L-ArgDH has *Pro*-R specificity similar to L-AlaDH for the hydride transfer to $NADP^+$. As proposed for the L-alanine molecule modeled into the *A. fulgidus* L-AlaDH structure, the carboxylate group of L-arginine interacts with the side chain of Arg111 (Fig. 4), which corresponds to Arg108 in *A. fulgidus* L-AlaDH but not in a bidentate manner. The carboxylate group is also recognized by the side chain of Lys71, corresponding to Lys65 in the *A. fulgidus* enzyme. The α-amino group of L-arginine forms hydrogen bonds with the side chains of Thr224 and Asn225. The amino acid residues corresponding to these two residues are not present in *A. fulgidus* L-AlaDH

(Supplementary Fig. 2A). The guanidino group of the substrate L-arginine hydrogen bonded to the side chain of Asp54 and the main chain O atom of Ser73 (Supplementary Table 2). To assess the role of Asp54, we constructed a D54A mutant and observed that the specific activity of the mutant was only about 1.8% of the wild-type enzyme activity, which suggests recognition of the L-arginine guanidino group by the Asp54 side chain is essential for maintaining high reactivity for L-arginine.

3.5. Comparison with OCD

On searching for proteins with similar structures using the DALI server [30], the OCD from *P. putida* [PDB code: 1X7D (NADH/L-ornithine-bound structure) [15] showed high structural similarity with *P. veronii* L-ArgDH (r.m.s.d. = 2.4-2.5). In *P. putida* OCD, the L-ornithine molecule exhibits a binding mode similar to that observed for the L-arginine molecule in *P. veronii* L-ArgDH (Fig. 5A, B), although the side chain of L-ornithine takes an alternative conformation with an occupancy of 0.5. Within this structure, the carboxylate group of L-ornithine was recognized by the side chains of Arg45, Lys69, and Arg112. Among these residues, Lys69 and Arg112 are respectively conserved as Lys71 and Arg111 in *P. veronii* L-ArgDH (Supplementary Fig. 2B). The α-amino group of L-ornithine donates a hydrogen bond to the side chain of Asp228, and this side chain

functions as a proton acceptor that facilitates the formation of the imino substituent [15]. In *P. veronii* L-ArgDH, as described above, the α-amino group of L-arginine interacts with the side chains of Thr224 and Asn225, which occupy the vicinal position of the side chain of Asp228 in *P. putida* OCD. To examine the roles of Thr224 and Asn225, we constructed T224A and N225A mutants and observed that the N225A substitution had little effect on the specific activity of the enzyme, whereas the specific activity of the T224A mutant was dramatically reduced (about 0.25% of the wild-type V_{max} value). Although the reaction rate was low, the T224A mutant retained catalytic activity, suggesting Thr224 is not essential for catalysis. Recognition of the α-amino group of L-arginine by the side chains of Thr224 and Asn225 may occur, particularly within the active site of the abortive complex of the enzyme with substrate L-arginine and product NADPH bound.

3.6. Insight into the reaction mechanism

A preliminary outline of the reaction mechanism based on the model of *A. fulgidus* L-AlaDH with L-alanine bound was previously reported [11]. As described above, the α-amino group of L-alanine modeled into the *A. fulgidus* enzyme formed a hydrogen bond with a water molecule (W510), which was also hydrogen bonded with the side chains of Lys41 and Arg52 (Fig. 4). Consequently, W510 was thought to mediate proton transfer

for catalysis [11]. However, the amino acid residues and a water molecule corresponding to those two residues and W510 were not observed in *P. veronii* L-ArgDH.

In the reaction of amino acid dehydrogenases, which catalyze $NAD(P)^+$-dependent dehydrogenation at the Cα position of amino acids accompanied by deamination, the α-amino group (α-keto group in the reverse reaction) of the substrate requires an acid/base capable of catalytically transferring protons. This role is played by His in *Phormidium* L-AlaDH [1] and by Lys in *Rhodococcus* L-PheDH [4]. In *P. veronii* L-ArgDH, no His residue is observed within 5 Å of the substrate Cα, but Lys71 is located within 5 Å. In the above L-AlaDH and L-PheDH, the catalytic acid/base functional group, whether His or Lys, has an Asp or Glu residue as a partner. This appears to be Asp303 in *P. veronii* L-ArgDH, which is within 3 Å of Lys 71 (Fig. 4). The residues corresponding to Lys71 and Asp303 are conserved among the homologs of *P. veronii* L-ArgDH (Supplementary Figure 5) [14], suggesting that Lys71 acts as the catalytic acid/base in L-ArgDHs as predicted for *A. fulgidus* L-AlaDH [11].

As shown in Fig. 4, on the other hand, the side chain of Tyr58 (OH) is located nearby the substrate Cα (about 4 Å) in *P. veronii* L-ArgDH and it forms a triad with the side chains of Lys71 (NZ) and Ser73 (OG). In short-chain dehydrogenase/reductase family enzymes, the Ser-Tyr-Lys catalytic triad is essential for catalysis. The side-chain oxygen

of the Tyr residue functions as an acid/base catalyst for proton transfer, and the Ser residue plays a secondary role in the stabilization of substrate binding [31]. The Lys residue has two critical roles: it interacts with the OH groups of the nicotinamide ribose (cofactor binding) and lowers the p*Ka* value of the OH group in the side chain of the Tyr residue [31]. In L-ArgDHs, therefore, Tyr58 may serve as the acid/base catalytic residue instead of Lys71. To examine the role of Tyr58 and Lys71, we constructed Y58F and K71A mutants and observed that these substitutions completely abolished enzyme activity. This indicates that Tyr58 and Lys71 play critical roles in enzyme catalysis. The residues corresponding to Tyr58, Lys71, and Ser73 in *P. veronii* L-ArgDH are completely conserved among the L-ArgDH homologs (Supplementary Figure 5) [14], though Tyr58 and Ser73 are respectively replaced by Met and Val in *A. fulgidus* L-AlaDH and *P. putida* OCD (Supplementary Figure 2). In particular, the Tyr58 in the active site of *P. veronii* L-ArgDH may be a benchmark that distinguishes L-ArgDHs from L-AlaDHs/OCDs in the μ-crystallin/OCD family, although further experimental verification should be necessary.

4. Conclusions

In the present study, we determined the crystal structures of *P. veronii* L-ArgDH with L-lysine and coenzyme $NADP^+$ bound as well as with its natural substrate, L-arginine,

and NADPH bound. The substrate recognition residues differed from those of *A. fulgidus* L-AlaDH. Asp54 plays a critical role in maintaining high reactivity against the substrate L-arginine. In addition, Tyr58 and Lys71 were found to play critical roles in enzyme catalysis. The Tyr58 in the active site of *P. veronii* L-ArgDH may serve as a criterion for distinguishing L-ArgDHs from L-AlaDHs. These findings will facilitate a better understanding of the structure-function relationships within amino acid dehydrogenases belonging to the μ-crystallin/OCD family.

The following are the supplementary data related to this article.

Supplementary Table 1.

Primer sequences for site-directed mutagenesis

Supplementary Table 2.

Descriptive table of the observed hydrogen bonds between the enzyme and coenzyme/substrates.

Supplementary Fig. 1.

Stereographic close-up of subunit B of *P. veronii* L-ArgDH with L-lysine/$NADP^+$ bound.

Supplementary Fig. 2

Structure-based amino acid sequence alignments of *P. veronii* L-ArgDH (ArgDH), *A. fulgidus* L-AlaDH (AlaDH), and *P. putida* OCD (OCD).

Supplementary Fig. 3

Comparison of the modes of cofactor binding to *P. veronii* L-ArgDH subunit B with L-lysine/$NADP^+$ bound and subunit D with $NADP^+$ bound.

Supplementary Fig. 4

Stereographic close-up of *P. veronii* L-ArgDH with L-arginine/NADPH bound.

Supplementary Figure 5

Amino acid sequence alignments of L-ArgDH homologs.

Acknowledgments

We are grateful to the staff of the Photon Factory for their assistance with data collection, which was approved by the Photon Factory Program Advisory Committee. This work was supported in part by research funds from the Public Utility Foundation for the Vitamin & Biofactor Society (to H. S.) and the Japan Society for the Promotion of Science (KAKENHI grant No. 23K05658 to H. S., 20K05729 to R.K., and 20K05816 to To. O.).

Footnotes

Abbreviations: L-AlaDH, L-alanine dehydrogenase; L-ArgDH, L-arginine dehydrogenase; ELFVW glutamate, leucine, phenylalanine, valine, and tryptophan dehydrogenases; OCD, ornithine cyclodeaminase; PEG, polyethylene glycol; PDB, Protein Data Bank; ASA, accessible surface area; r.m.s.d., root-mean-square deviation.

Author contributions

HS supervised the project; NT performed crystallographic experiments; HS, NT, and JH performed data collection and model building; RK, NT, and TO performed biochemical assays; RK, NT, KY, ToO, and HS analyzed data and prepared the manuscript. All authors approved the submitted and published versions of the manuscript.

Conflict of interest

The authors declare no conflicts of interest.

Ethical statement

This article does not contain any studies with human participants or animals performed by any of the authors.

Figure legends

Fig. 1. Overall structure of *P. veronii* L-ArgDH with L-lysine and $NADP^+$ bound. Binding of both the L-lysine and $NADP^+$ molecules is observed only in subunit B. The structures of subunits A and D are the $NADP^+$-bound forms, while that of subunit C is the L-lysine/$NADP^+$-unbound form. L-lysine and $NADP^+$ molecules are shown in magenta and yellow, respectively. The smaller dimerization/catalytic domain 1 and the larger NADP-binding domain 2 of subunit A are shown.

Fig. 2. *A*, Stereographic close-up of $NADP^+$ bound to subunit D of *P. veronii* L-ArgDH. Residues surrounding the $NADP^+$ molecule are shown in green. $NADP^+$ is shown in magenta. *B*, Stereographic close-up of the adenine and adenine ribose moieties of NAD^+ bound to *A. fulgidus* L-AlaDH. The networks of hydrogen bonds are shown as dashed lines.

Fig. 3. Comparison of the active site structures in subunit B of *P. veronii* L-ArgDH with L-lysine/$NADP^+$ bound (green and red labels) and *A. fulgidus* L-AlaDH with NAD^+ bound (cyan and black labels) (stereo representation). $NADP^+$, L-lysine, and water (W200) in *P. veronii* L-ArgDH are shown in magenta, yellow, and red, respectively. NAD^+ and water

(W510) in *A. fulgidus* L-AlaDH are shown in orange and gray, respectively. The networks of hydrogen bonds are shown as dashed lines.

Fig. 4. Comparison of the active site structures in *P. veronii* L-ArgDH with L-arginine/NADPH bound (green and red labels) and *A. fulgidus* L-AlaDH with NAD^+ bound (cyan and black labels) (stereo representation). NADPH and L-arginine in *P. veronii* L-ArgDH are shown in magenta and yellow, respectively. NAD^+ and water (W510) in *A. fulgidus* L-AlaDH are shown in orange and gray, respectively. The networks of hydrogen bonds are shown as dashed lines.

Fig. 5. *A*, Stereographic close-up of the L-ornithine binding site in *P. putida* OCD (cyan). L-Ornithine is shown in yellow. *B*, Stereographic close-up of the L-arginine binding site in *P. veronii* L-ArgDH (green). L-Arginine is shown in yellow. The networks of hydrogen bonds are shown as dashed lines.

References

[1] P.J. Baker, Y. Sawa, H. Shibata, S.E. Sedelnikova, D.W. Rice, Analysis of the structure and substrate binding of *Phormidium lapideum* alanine dehydrogenase, Nat. Struct. Biol. 5 (1998) 561-567. https://doi.org/10.1038/817.

[2] T.J. Stillman, P.J. Baker, K.L. Britton, D.W. Rice, Conformational flexibility in glutamate dehydrogenase: Role of water in substrate recognition and catalysis, J. Mol. Biol. 234 (1993) 1131-1139. https://doi.org/10.1006/jmbi.1993.1665

[3] P.J. Baker, A.P. Turnbull, S.E. Sedelnikova, T.J. Stillman, D.W. Rice, A role for quaternary structure in the substrate specificity of leucine dehydrogenase, Structure 3 (1995) 693-705. https://doi.org/10.1016/s0969-2126(01)00204-0

[4] J.L. Vanhooke, J.B. Thoden, N.M. Brunhuber, J.S. Blanchard, H.M. Holden, Phenylalanine dehydrogenase from *Rhodococcus* sp. M4: High-resolution X-ray analyses of inhibitory ternary complexes reveal key features in the oxidative deamination mechanism, Biochemistry (Mosc). 38 (1999) 2326-2339. https://doi.org/10.1021/bi982244q

[5] L. Tang, C.R. Hutchinson, Sequence, transcriptional, and functional analyses of the valine (branched-chain amino acid) dehydrogenase gene of *Streptomyces coelicolor*, J. Bacteriol. 175 (1993) 4176-4185. https://doi.org/10.1128/jb.175.13.4176-4185.1993

[6] R. Ogura, T. Wakamatsu, Y. Mutaguchi, K. Doi, T. Ohshima, Biochemical characterization of an L-tryptophan dehydrogenase from the photoautotrophic cyanobacterium *Nostoc punctiforme*, Enzyme Microb. Technol. 60 (2014) 40-64. https://doi.org/10.1016/j.enzmictec.2014.04.002

[7] T. Wakamatsu, H. Sakuraba, M. Kitamura, Y. Hakumai, K. Fukui, K. Ohnishi, M. Ashiuchi, T. Ohshima, Structural insights into L-tryptophan dehydrogenase from a photoautotrophic cyanobacterium, *Nostoc punctiforme*, Appl. Environ. Microbiol. 83 (2017) e02710-16. https://doi.org/10.1128/AEM.02710-16

[8] Z. Yang, A. Savchenko, A. Yakunin, R. Zhang, A. Edwards, C. Arrowsmith, L. Tong, Aspartate dehydrogenase, a novel enzyme identified from structural and functional studies of TM1643, J. Biol. Chem. 278 (2003) 8804-8808. https://doi.org/10.1074/jbc.M211892200

[9] K. Yoneda, R. Kawakami, Y. Tagashira, H. Sakuraba, S. Goda, T. Ohshima, The first

archaeal L-aspartate dehydrogenase from the hyperthermophile *Archaeoglobus fulgidus*: gene cloning and enzymological characterization, Biochim. Biophys. Acta 1764 (2006) 1087-1093. https://doi.org/ 10.1016/j.bbapap.2006.04.006.

[10] K. Yoneda, H. Sakuraba, H. Tsuge, N. Katunuma, T. Ohshima, Crystal structure of archaeal highly thermostable L-aspartate dehydrogenase/NAD/citrate ternary complex, FEBS J 274 (2007) 4315-4325. https://doi.org/10.1111/j.1742-4658.2007.05961.x

[11] D.T. Gallagher, H.G. Monbouquette, I. Schroder, H. Robinson, M.J. Holden, N.N. Smith, Structure of alanine dehydrogenase from *Archaeoglobus*: active site analysis and relation to bacterial cyclodeaminases and mammalian mu crystallin, J. Mol. Biol. 342 (2004) 119-130. https://doi.org/10.1016/j.jmb.2004.06.090

[12] I. Schroder, A. Vadas, E. Johnson, S. Lim, H.G. Monbouquette, A novel archaeal alanine dehydrogenase homologous to ornithine cyclodeaminase and μ-crystallin, J. Bacteriol. 186 (2004) 7680-7689. https://doi.org/10.1128/JB.186.22.7680-7689.2004

[13] C. Li, C.D. Lu, Arginine racemization by coupled catabolic and anabolic

dehydrogenases, Proc. Natl. Acad. Sci. U. S. A. 106 (2009) 906-911.
https://doi.org/10.1073/pnas.0808269106
[14] T. Ohshima, M. Tanaka, T. Ohmori, $NADP^+$-dependent L-arginine dehydrogenase from *Pseudomonas veronii*: Purification, characterization and application to an L-arginine assay, Protein Expr. Purif. 199 (2022) 106135.
https://doi.org/10.1016/j.pep.2022.106135
[15] J.L. Goodman, S. Wang, S. Alam, F.J. Ruzicka, P.A. Frey, J.E. Wedekind, Ornithine cyclodeaminase: structure, mechanism of action, and implications for the μ-crystallin family, Biochemistry (Mosc). 43 (2004) 13883-13891.
https://doi.org/10.1021/bi048207i
[16] W. Kabsch, Xds, Acta Crystallogr. D Biol. Crystallogr. 66 (2010) 125-132.
https://doi.org/10.1107/S0907444909047337
[17] P.R. Evans, G.N. Murshudov, How good are my data and what is the resolution?, Acta Crystallogr. D Biol. Crystallogr. 69 (2013) 1204-1214.
https://doi.org/10.1107/S0907444913000061
[18] M.D. Winn, C.C. Ballard, K.D. Cowtan, E.J. Dodson, P. Emsley, P.R. Evans, R.M. Keegan, E.B. Krissinel, A.G. Leslie, A. McCoy, S.J. McNicholas, G.N. Murshudov, N.S. Pannu, E.A. Potterton, H.R. Powell, R.J. Read, A. Vagin, K.S. Wilson, Overview of the

CCP4 suite and current developments, Acta Crystallogr. D Biol. Crystallogr. 67 (2011) 235-242.
https://doi.org/10.1107/S0907444910045749
[19] A. Vagin, A. Teplyakov, Molecular replacement with MOLREP, Acta Crystallogr. D Biol. Crystallogr. 66 (2010) 22-25.
https://doi.org/10.1107/S0907444909042589
[20] J. Jumper, R. Evans, A. Pritzel, T. Green, M. Figurnov, O. Ronneberger, K. Tunyasuvunakool, R. Bates, A. Zidek, A. Potapenko, A. Bridgland, C. Meyer, S.A.A. Kohl, A.J. Ballard, A. Cowie, B. Romera-Paredes, S. Nikolov, R. Jain, J. Adler, T. Back, S. Petersen, D. Reiman, E. Clancy, M. Zielinski, M. Steinegger, M. Pacholska, T. Berghammer, S. Bodenstein, D. Silver, O. Vinyals, A.W. Senior, K. Kavukcuoglu, P. Kohli, D. Hassabis, Highly accurate protein structure prediction with AlphaFold, Nature 596 (2021) 583-589.
https://doi.org/10.1038/s41586-021-03819-2
[21] P. Emsley, B. Lohkamp, W.G. Scott, K. Cowtan, Features and development of Coot, Acta Crystallogr. D Biol. Crystallogr. 66 (2010) 486-501.
https://doi.org/10.1107/S0907444910007493
[22] G.N. Murshudov, P. Skubak, A.A. Lebedev, N.S. Pannu, R.A. Steiner, R.A. Nicholls,

M.D. Winn, F. Long, A.A. Vagin, REFMAC5 for the refinement of macromolecular crystal structures, Acta Crystallogr. D Biol. Crystallogr. 67 (2011) 355-367. https://doi.org/10.1107/S0907444911001314

[23] S.C. Lovell, I.W. Davis, W.B. Arendall, 3rd, P.I. de Bakker, J.M. Word, M.G. Prisant, J.S. Richardson, D.C. Richardson, Structure validation by Cα geometry: ϕ, ψ and Cβ deviation, Proteins 50 (2003) 437-450. https://doi.org/10.1002/prot.10286

[24] E. Krissinel, K. Henrick, Inference of macromolecular assemblies from crystalline state, J. Mol. Biol. 372 (2007) 774-797. https://doi.org/10.1016/j.jmb.2007.05.022

[25] S. McNicholas, E. Potterton, K.S. Wilson, M.E. Noble, Presenting your structures: the CCP4mg molecular-graphics software, Acta Crystallogr. D Biol. Crystallogr. 67 (2011) 386-394. https://doi.org/10.1107/S0907444911007281

[26] E. Krissinel, K. Henrick, Secondary-structure matching (SSM), a new tool for fast protein structure alignment in three dimensions, Acta Crystallogr. D Biol. Crystallogr. 60 (2004) 2256-2268. https://doi.org/10.1107/S0907444904026460

[27] D. Liebschner, P.V. Afonine, N.W. Moriarty, B.K. Poon, O.V. Sobolev, T.C. Terwilliger, P.D. Adams, Polder maps: improving OMIT maps by excluding bulk solvent, Acta Crystallogr. D Struct. Biol. 73 (2017) 148-157. https://doi.org/10.1107/S2059798316018210

[28] P.D. Adams, P.V. Afonine, G. Bunkoczi, V.B. Chen, I.W. Davis, N. Echols, J.J. Headd, L.W. Hung, G.J. Kapral, R.W. Grosse-Kunstleve, A.J. McCoy, N.W. Moriarty, R. Oeffner, R.J. Read, D.C. Richardson, J.S. Richardson, T.C. Terwilliger, P.H. Zwart, PHENIX: a comprehensive Python-based system for macromolecular structure solution, Acta Crystallogr. D Biol. Crystallogr. 66 (2010) 213-221. https://doi.org/10.1107/S0907444909052925

[29] B.W. Matthews, Solvent content of protein crystals, J. Mol. Biol. 33 (1968) 491-497. https://doi.org/10.1016/0022-2836(68)90205-2.

[30] L. Holm, P. Rosenström, Dali server: conservation mapping in 3D, Nucleic Acids Res. 38 (2010) W545-W549. https://doi.org/10.1093/nar/gkq366

[31] K.L. Kavanagh, H. Jornvall, B. Persson, U. Oppermann, Medium- and short-chain dehydrogenase/reductase gene and protein families: The SDR superfamily: functional and structural diversity within a family of metabolic and regulatory enzymes, Cell. Mol.

1 Life Sci. 65 (2008) 3895-3906.

2 https://doi.org/10.1007/s00018-008-8588-y

3 [32] J.D. Thompson, D.G. Higgins, T.J. Gibson, CLUSTAL W: improving the sensitivity

4 of progressive multiple sequence alignment through sequence weighting, position-

5 specific gap penalties and weight matrix choice, Nucleic Acids Res. 22 (1994) 4673-4680.

6 https://doi.org/10.1093/nar/22.22.4673

7

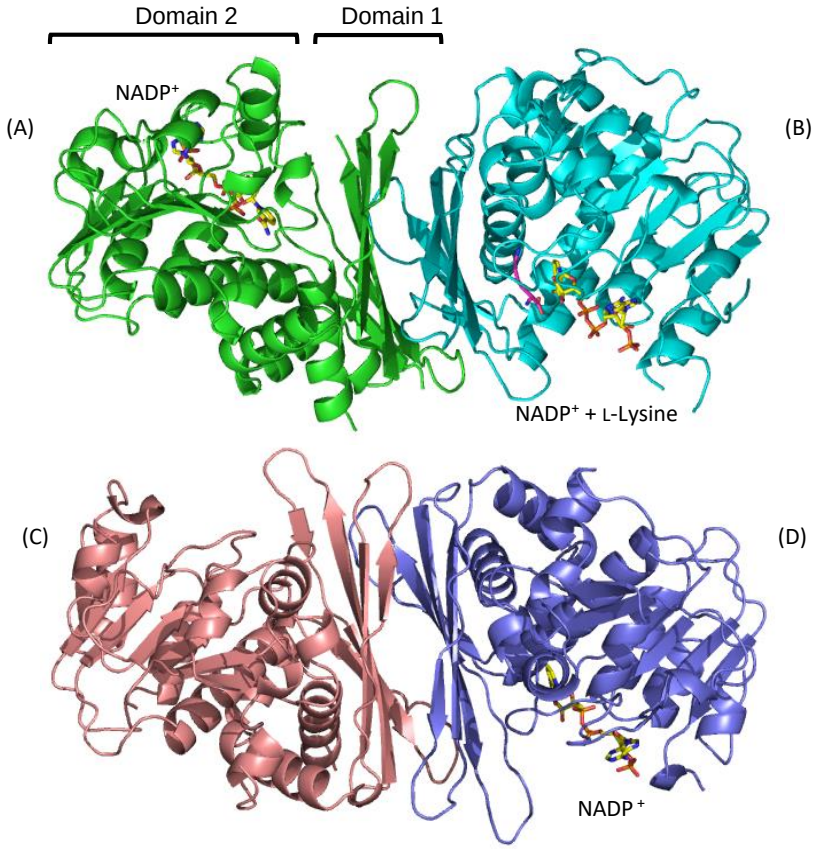

Fig. 1

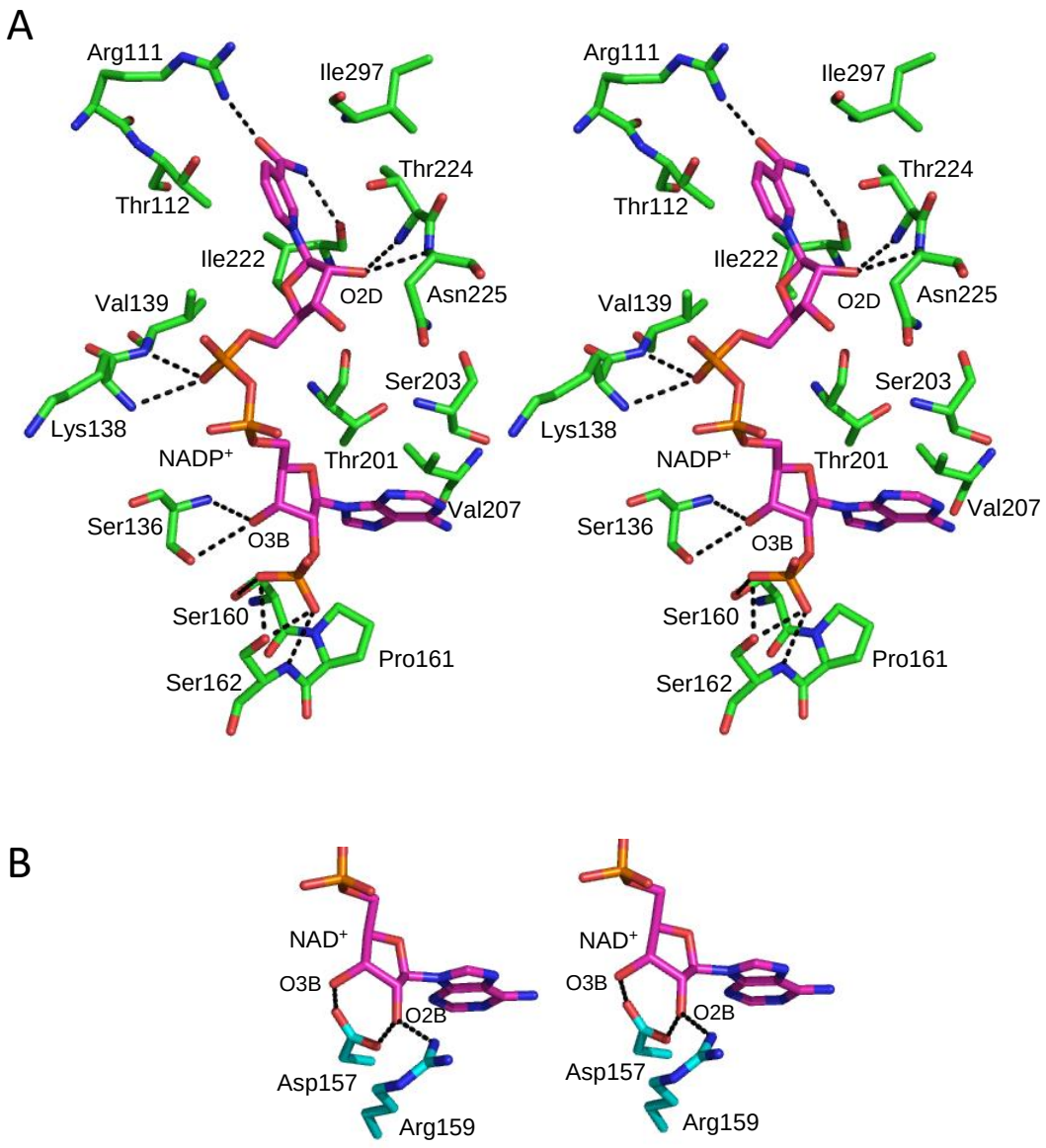
A
Arg111
Ile297
Thr224
Thr112
Ile222
O2D
Asn225
Val139
Ser203
Lys138
NADP+
Thr201
Val207
Ser136
O3B
Ser160
Pro161
Ser162
Arg111
Ile297
Thr224
Thr112
Ile222
O2D
Asn225
Val139
Ser203
Lys138
NADP+
Thr201
Val207
Ser136
O3B
Ser160
Pro161
Ser162
B
NAD+
O3B
O2B
Asp157
Arg159
NAD+
O3B
O2B
Asp157
Arg159

Fig. 2

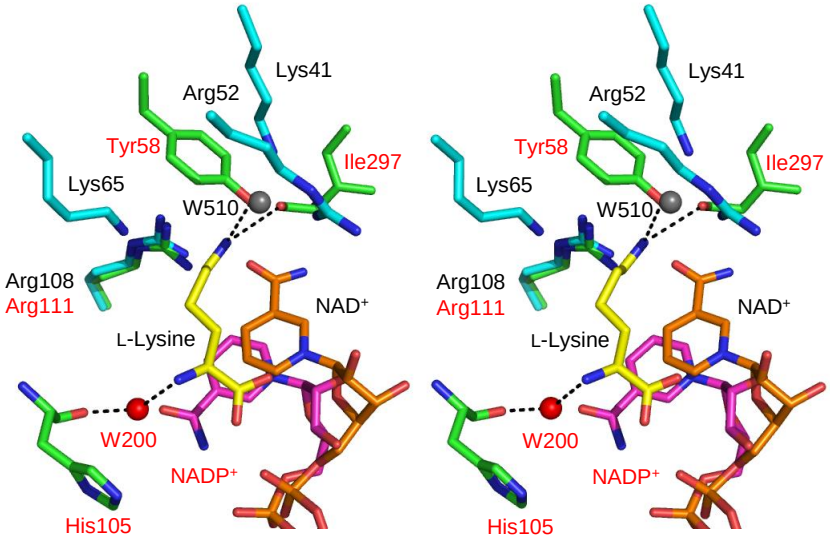
Lys41
Arg52
Tyr58
Ile297
Lys65
W510
Arg108
Arg111
NAD+
L-Lysine
W200
NADP+
His105
Lys41
Arg52
Tyr58
Ile297
Lys65
W510
Arg108
Arg111
NAD+
L-Lysine
W200
NADP+
His105

Fig. 3

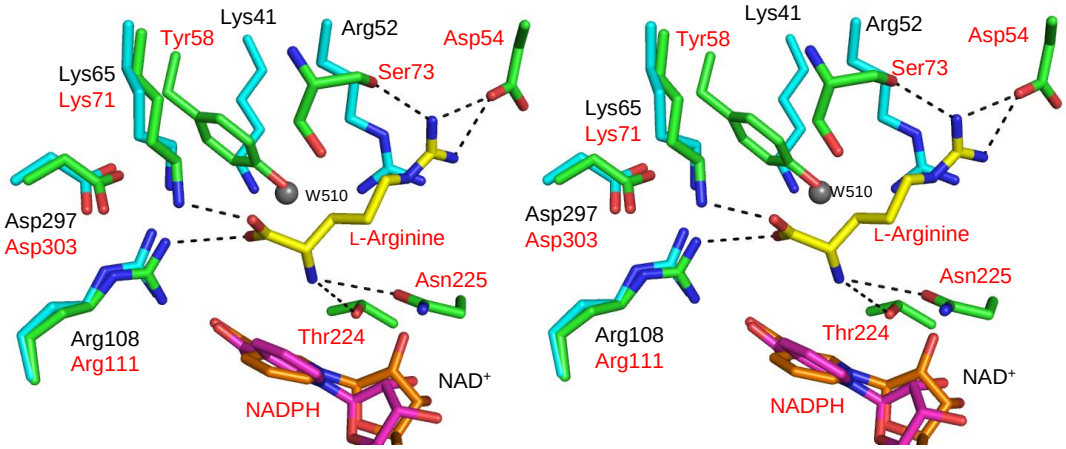
Lys41
Tyr58
Arg52
Asp54
Lys65
Lys71
Ser73
W510
Asp297
Asp303
L-Arginine
Asn225
Arg108
Arg111
Thr224
NAD+
NADPH
Lys41
Tyr58
Arg52
Asp54
Lys65
Lys71
Ser73
W510
Asp297
Asp303
L-Arginine
Asn225
Arg108
Arg111
Thr224
NAD+
NADPH

Fig. 4

A

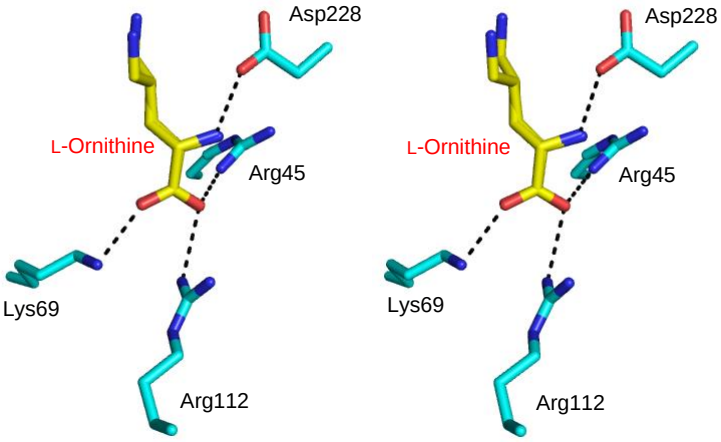
Asp228
L-Ornithine
Arg45
Lys69
Arg112
Asp228
L-Ornithine
Arg45
Lys69
Arg112

B

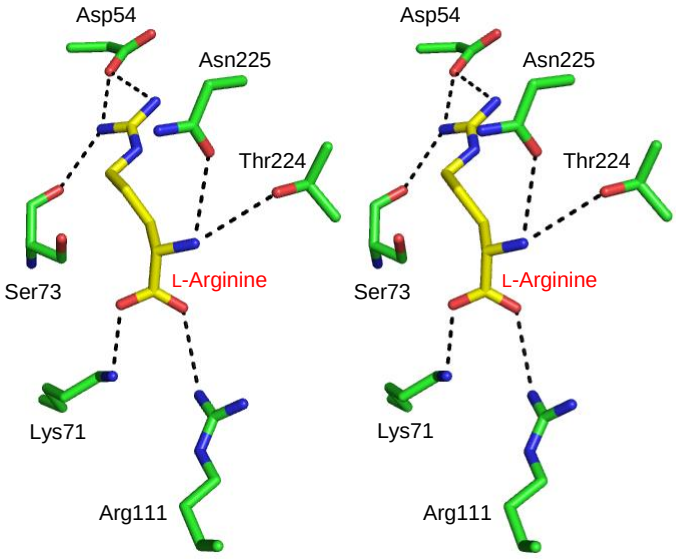
Asp54
Asn225
Thr224
Ser73
L-Arginine
Lys71
Arg111
Asp54
Asn225
Thr224
Ser73
L-Arginine
Lys71
Arg111

Fig. 5

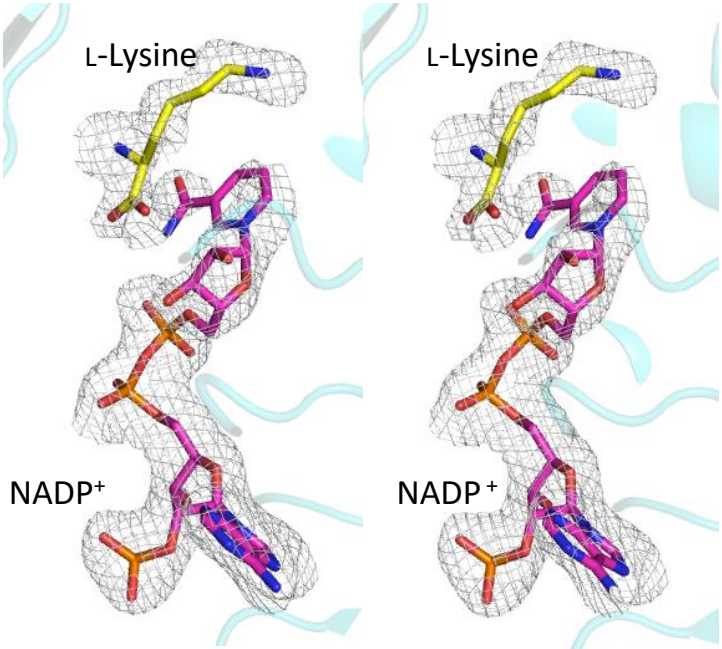

Supplementary Figure 1.

Stereographic close-up of subunit B of *P. veronii* L-ArgDH with L-lysine/$NADP^+$ bound. $NADP^+$ and L-lysine are shown in magenta and yellow, respectively. The final Fo - Fc omit electron density map for $NADP^+$ and L-lysine was generated using Polder Maps [23] (contoured at 3.5σ).

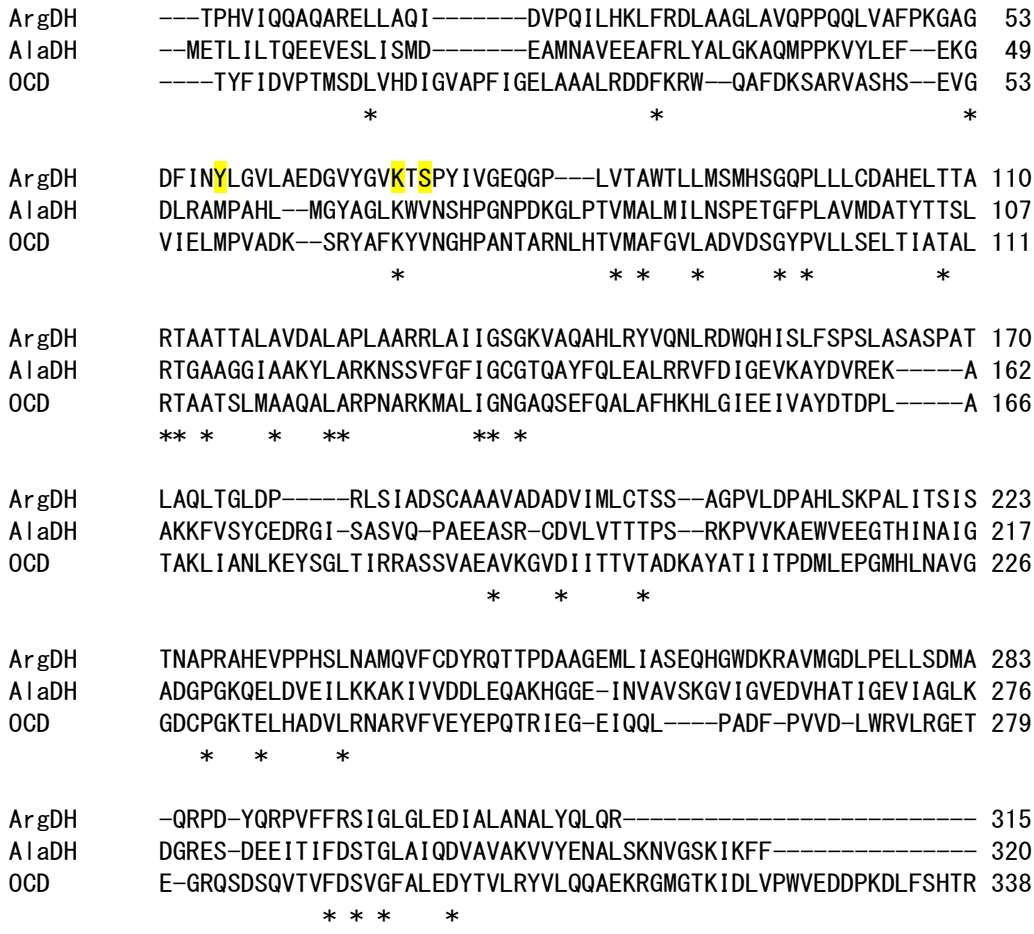

Supplementary Figure 2.

Structure-based amino acid sequence alignments of *P. veronii* L-ArgDH (ArgDH), *A. fulgidus* L-AlaDH (AlaDH), and *P. putida* OCD (OCD). Sequences were aligned using the DALI server [30]. Asterisks indicate conserved residues. Tyr58, Lys71, and Ser73 in *P. veronii* L-ArgDH are shown on a yellow background.

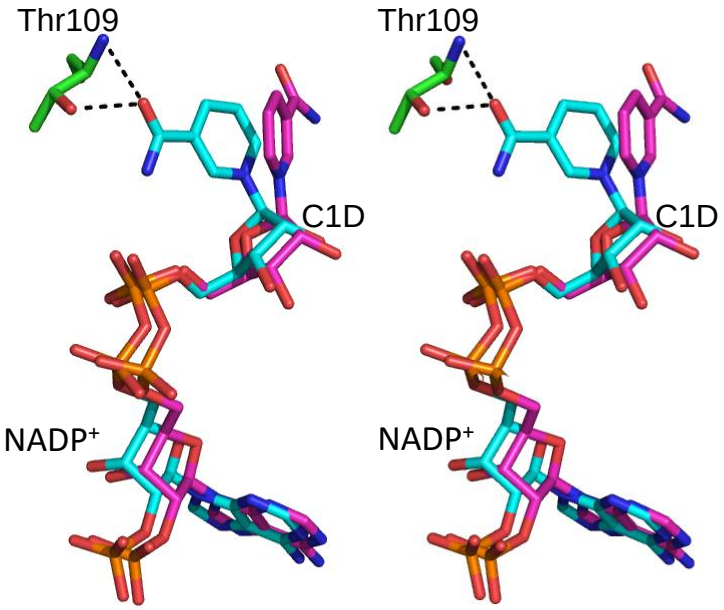

Supplementary Figure 3.

Comparison of the modes of cofactor binding to *P. veronii* L-ArgDH subunit B with L-lysine/$NADP^+$ bound and subunit D with $NADP^+$ bound. $NADP^+$ molecules in subunits B and D are shown in cyan and magenta, respectively.

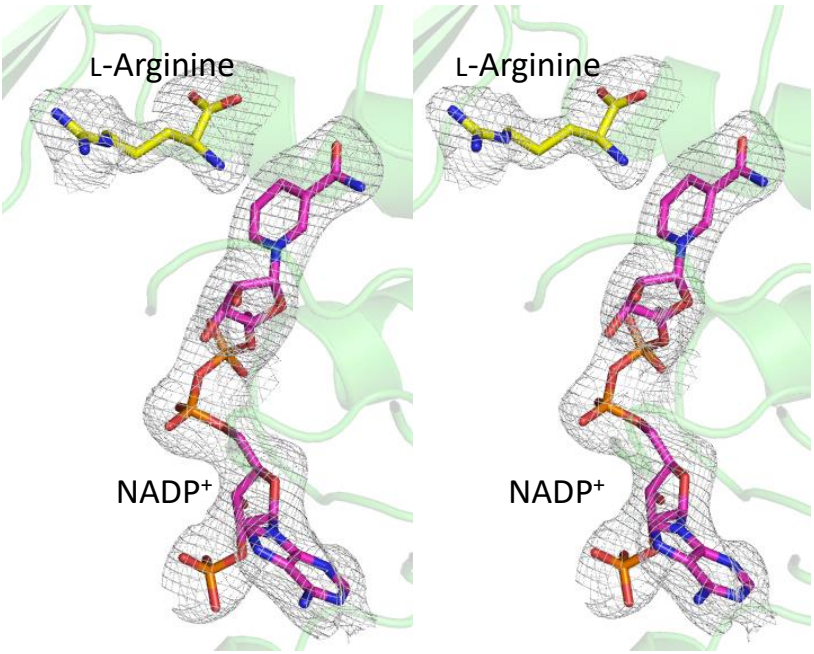

Supplementary Figure 4.

Stereographic close-up of *P. veronii* L-ArgDH with L-arginine/NADPH bound. NADPH and L-arginine are shown in magenta and yellow, respectively. The final Fo - Fc omit electron density map for NADPH and L-arginine was generated using Polder Maps [23] (contoured at 3.5σ).

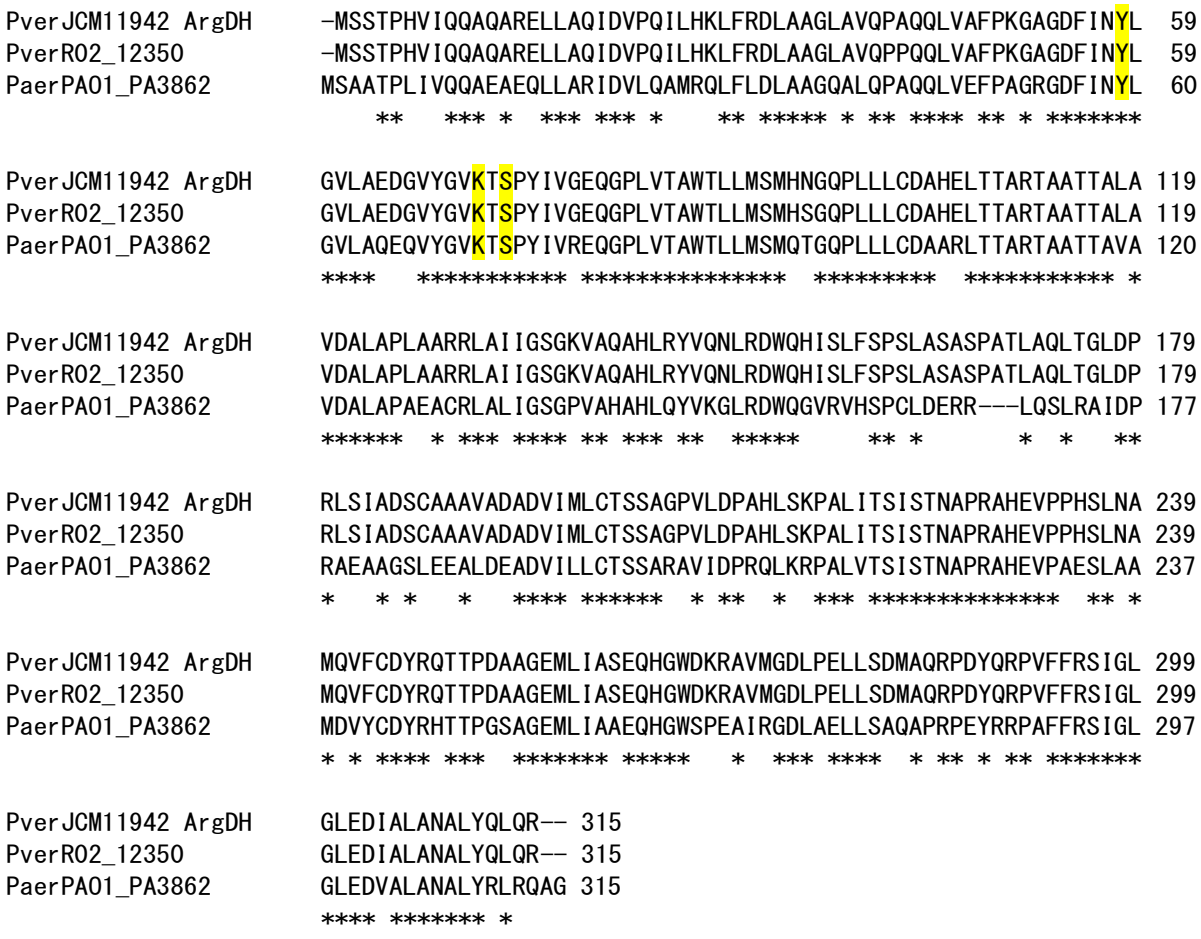

Supplementary Figure 5

Amino acid sequence alignments of L-ArgDH homologs.
PverJCM11942 ArgDH, *P. veronii* L-ArgDH, PverR02_12350, *P. veroni* putative L-ArgDH [14], and PaerPAO1_PA3862, *P. aeruginosa* L-ArgDH. Sequences were aligned using Clustal W [32]. Asterisks indicate conserved residues. The putative Ser-Tyr-Lys triad is shown on a yellow background.

Supplementary Table 1.

Sequences of primers used for site-directed mutagenesis.

D54A_Fw	GGTAGTTGATGAAGGCGCCGGCGCCCTT
D54A_Rv	AAGGGCGCCGGCGCCTTCATCAACTACC
Y58F_Fw	GCCGGCGACTTCATCAACTTCCTGGGCGTG
Y58F_Rv	CACGCCCAGGAAGTTGATGAAGTCGCCGGC
K71A_Fw	ATGTACGGCGAAGTCGCGACCCCGTACACGCC
K71A_Rv	GGCGTGTACGGGGTCGCGACTTCGCCGTACAT
T224A_Fw	CGGGGCGCATTGGCGCTGATCGAAGTG
T224A_Rv	CACTTCGATCAGCGCCAATGCGCCCCG
N225A_Fw	ATGGGCGCGGGGCGCCGCGGTGCTGATCGAAGT
N225A_Rv	ACTTCGATCAGCACCGCGGCGCCCCGCGCCCAT

Supplementary Table 2

Descriptive table of the observed hydrogen bonds between enzyme and coenzyme/substrates.

Atoms participating in the hydrogen interactions				
			Distance (Å)	
$NADP^+$ (Subunit D)	Adenine ribose phosphate	O2X	3.32	Ser160 OG
			2.72	Ser162 OG
		O3X	2.60	Ser162 OG
			2.98	Ser162 N
	Adenine ribose	O3B	3.20	Ser136 OG
			3.05	Ser136 N
	Pyrophosphate	O2N	3.14	Lys138 N
			3.01	Val139 N
	Nicotinamide ribose	O2D	2.80	Thr224 N
			2.81	Asn225 N
	Nicotinamide	O7N	2.71	Arg111 NH1
		N7N	2.83	Ile222 O
L-Lysine (subunit B)	Epsilon amino group	NZ	2.97	Tyr58 OH
			3.38	Ile297 O
	Alpha amino group	N	2.58	Wat200
	Wat200	O	2.66	His105 O
L-Arginine	Carboxylate group	O	3.24	Arg111 NH2
		OXT	2.70	Lys71 NZ
	Alpha amino group	N	3.44	Thr224 OG1
			3.29	Asn225 OD1
	Guanidino group	NH1	2.60	Asp54 OD1
			2.91	Ser73 O
		NH2	2.77	Asp54 OD1

Table 1. Data-collection and refinement statistics.

	L-Lysine/$NADP^+$-bound L-ArgDH	L-Arginine/NADPH-bound L-ArgDH
PDB code	8J1C	8J1G
Data collection		
Synchrotron light source	Photon Factory	Photon Factory
Beamline	BL-5A	BL-5A
Wavelength (Å)	1.0	1.0
No. of frames	180	720
Oscillation width (deg)	1.0	1.0
Detector distance (mm)	429.05	451.90
Exposure per frame (s)	1	1
Temperature (K)	100	100
Indexing and scaling		
Space group	$P2_12_12_1$	$P1$
Unit cell parameters		
a (Å)	91.1	63.5
b (Å)	92.6	70.3
c (Å)	162.5	100.1
α (°)	90	89
β (°)	90	73
γ (°)	90	87
Resolution range (Å) [a]	46.7–2.20 (2.25–2.20)	47.8–2.50 (2.57–2.50)
Total No. of reflections	474464	393701
No. of unique reflections	70419	56308
Redundancy [a]	6.7 (7.0)	7.0 (6.7)
Completeness (%)[a]	100 (100)	98.7 (98.1)
$< I/\sigma(I) >$ [a]	16.8 (1.7)	18.9 (1.8)
R_{pim} [a, b]	0.030 (0.49)	0.026 (0.50)
$CC_{1/2}$ [a, c]	0.992 (0.730)	0.999 (0.657)
No. of chains per asymmetric unit	4	4
Refinement		
Resolution range (Å)	46.7–2.20	47.8–2.50

R/R_{free} (%) [a, d]	21.3/26.0	22.5/27.4
	(30.7/35.1)	(34.1/38.3)
No. of protein atoms	9119	9200
No. of water molecules	233	45
No. of ligands	Ethylene glycol, 1	Ethylene glycol, 2
	Imidazole, 3	NADPH, 4
	$NADP^+$, 3	L-Arginine, 4
	L-Lysine, 1	
Average B-factors (Å^2)	41.9	57.2
R.m.s.d.		
Bond lengths (Å)	0.006	0.007
Bond angles (°)	1.4	1.4
Ramachandran statistics		
Favored (%)	96.9	96.3
Allowed (%)	3.1	3.7
Outliers (%)	0	0

[a] Values in parentheses: highest resolution data shell; r.m.s.d.: root-mean-square deviation.

[b] $R_{pim} = \Sigma_h [1/ (/n_h - 1)]^{1/2} \Sigma_i | < I_h > - I_{h,i}| / \Sigma_h \Sigma_i I_{h,I}$, where h enumerates the unique reflections, i represents their symmetry-equivalent contributors, and n_h denotes multiplicity.

[c] $CC_{1/2}$ = Correlation between intensities from random half-data sets.

[d] R_{free} calculated with randomly selected reflections (5%).